ISSN: 2976-7466

Journal of Biosensors and Bioelectronics Research

SCIENTIFIC Research and Community

Research Article

Open Access

# Protein Complex Heterogeneity in the Nerve System

**Hengqi Wei, Ting Li and Congjian Zhao***

Chongqing University of Posts and Telecommunications, Chongqing, 400065, China

## ABSTRACT

A neuron has a unique axonal mRNA translocation and axonal translation. Thus, the neuron may have a different gene and protein expression regulation mechanism. However, we found that neuronal mRNA abundance is inverse-related to the CDS length of mRNA, which is consistent with other cell types. Meanwhile, the RNA and protein abundance have a low correlation, as revealed using paired mRNA-seq and proteomic data. Furthermore, our findings revealed the presence of extensive protein heterogeneity within main protein complexes. We utilized multiple single-cell mass spectrometry datasets to assess the protein heterogeneity within nuclear pore complexes and ribosomes. This study revealed a notable discrepancy between the proportion of protein complex subunits and their mature Stoichiometry under STED microscopy and CRYO-EM, suggesting heterogeneity of the protein complex.

***Corresponding author**

Congjian Zhao, Chongqing University of Posts and Telecommunications, Chongqing, 400065, China.

**Received:** June 03, 2025; **Accepted:** June 09, 2025; **Published:** June 17, 2025

## Introduction

Cellular function is contingent upon the accurate expression of proteins. The expression level of proteins is mainly regulated by their upstream regulation, including mRNA abundance and translation efficiency. A polarized neuron has multiple dendrites and a single long axon. mRNA transports from the soma to the distal axon and is translated locally. This mechanism resolves protein turnover at the distal synaptic terminal, creating a unique energy requirement and mRNA presence in the subcellular neuronal compartment. How is the mRNA abundance regulated in a neuron? Laura et al. observed a reverse relationship between mRNA abundance and gene length in T brucei [1]. This raises the question of whether mammalian neural tissue shares a similar mechanism.

Many housekeeping genes/proteins in neurons are stably expressed at the protein level, while some genes or proteins show transient expression upon neuronal activity. The ribosomes, a group of macromolecular complexes involved in protein translation, have demonstrated that these protein assembly machines are not passive and indiscriminate. Instead, they are dynamically assembled, forming different complexes to translate target proteins. Thus, it produces a variety of specialized ribosomes. Mass spectrometry results have identified a range of differential ribosomal protein abundance and species [2,3]. This suggests that the abundance of proteins in protein complexes fluctuates at a specific range related to the cellular states. We wanted to see whether this applies to neurons or how the heterogeneity of protein complexes in nerve tissue is.

In this study, using bioinformatics analysis of multiple datasets from various sources and with different methods, we studied the relationship between the mRNA abundance and gene length and the protein heterogeneity of protein complexes. The results demonstrate that the neuronal mRNA abundance exhibits an inverse relationship with the gene length. Moreover, we employed multiple paired transcriptome and mass spectrometry datasets to evaluate the heterogeneity of genes and proteins. Our data demonstrated the heterogeneity of protein complexes occurs at both mRNA and protein levels.

## Method

### Major Datasets Sources

RNA sequencing and mass spectrometry data were analyzed across species to assess the role of CDS length in mRNA abundance and protein expression in mammals. RNA-seq data and mass spectrometry data were retrieved from published work (Table 1).

**Table 1: Information and Sources of Data Sets for Analysis**

| Dataset title | Authors | Species | Dataset Accessibility | Application |
|---|---|---|---|---|
| Bulk RNA-seq | | | | |
| Axon bulk RNA-seq data in the CA1 region of the hippocampus | Zhuoxuan Y, Jun Y, Jian Z | Mus musculus | GSE201547 | Figure 1B, E |
| Long read ONT RNA-seq data of hippocampus | Emma FJ, Timothy CH, Victoria LF | Mus musculus | GSE246705 | Figure 1C, F |
| bulk RNA-seq data of neocortex | Maxime M, Katarzyna B, Peter S | Mus musculus | GSE210071 | Figure 1D, G; Figure 2A, D; Figure 3A, C, E |

| | | | | |
|---|---|---|---|---|
| Cerebral cortex bulk RNA-seq in human brain tissue | Mathias Uhlén | Homo sapiens | E-MTAB-2836 | Figure 2B, E; Figure 3A, C,E |
| Sc/sn RNA-seq | | | | |
| snRNA-seq data of hippocampal nuclei | Anoushka J, Wen H | Mus musculus | https://github.com/nou sh-joglekar/biccn_tilgner_s cisorseq/tree/main/data | Figure 1A, D |
| mice oocytes with complete GV stage and MII stage | Jiang YR, Zhu L, Cao LR | Mus musculus | GSE237932 | Figure 2C-D, 2G-H; Figure 3A, C, E |
| Bulk MS | | | | |
| Neocortex mass spectrometry of CD-1 mice | Dermot H, Mateusz C Ambrozkiewicz | Mus musculus | PXD014841 | Figure 3B, D, F |
| Cerebral cortex mass spectrometry in human brain tissue | Wang D, Eraslan B, Wieland T | Homo sapiens | PXD010154 | Figure 3B, D, F |
| Proteome analysis of A549 whole cell lysates | Edfors F, Danielsson F, Hallström BM | Homo sapiens | | Figure 4B, C, D |
| Proteome analysis of U2OS whole cell lysates | Beck M, Schmidt A, Malmstroem J | Homo sapiens | PXD000157 | Figure 4B, C, D |
| The relative expression ratio of RPs in cultured cortical neurons | Kirti S, Stefka T, Sebastian S | Homo sapiens | PXD001250 | Figure 4A |
| Single-cell MS | | | | |
| The workflow of single-cell protein analysis (PiSPA) is HeLa (scsp-504), A549 (scsp-503), and u2os (scsp-5030) cells. | Wang Y, Guan ZY, Shi SW | Homo sapiens | PXD041966 | Figure 4B, C, D |
| Proteochip Evo 96/ nanolute workflow: HEK293t by single cell protein analysis. | Ctortecka C, Clark NM, Boyle B | Homo sapiens | MSV000093867 | Figure 4B, C, D |
| Single-cell simultaneous transcription and protein groups (scSTAP) were analyzed for mice oocytes with complete GV and MII stages. | Jiang YR, Zhu L, Cao LR | Mus musculus | PXD043935 | Figure 3B, D, F |

**Bulk and Single-Cell RNA-Sequencing Data Mapping and Processing**

For the bulk RNA sequencing data analysis, raw sequencing reads were processed by Fastp and aligned onto the mouse reference genome (GRCh39, vM34) and human reference genome (GRCh38) using the STAR aligner version 2.7.10b. Then, read alignment bam files were processed with subread using the library feature Counts scripts. For the single-cell RNA sequencing data analysis, 10× matrix, barcode, and feature files were imported into R software (version 4.3.0) using the Seurat R package (version 5.1.0). After filtering according to the conditions of references, the expression matrix is derived.

**MaxQuant or DIA-NN Quantitative Mass Spectrometry Data**

The mass spectrometry data of human brain tissue (PXD010154) and mouse brain tissue (PXD014841) were quantified by MaxQuant (v2.6.1.0) or human reference genome (GRCh38) according to the methods in the literature. The single-cell mass spectrometry data of HEK293T cell (MSV000093867) were quantified by DIA-NN (v1.9.1) according to the methods in the literature. Other mass spectrometry data are from supplementary documents of references.

Analysis of Length and Abundance of Specific Protein Complexes

The gene list of protein complexes comes from the interactive protein websites CORUM and Complex Porta. The following protein complexes were selected from the websites: 40S ribosomal subunit, 60S ribosomal subunit, nuclear pore complex, 28S ribosomal subunit, mitochondrial, 39S ribosomal subunit, mitochondrial, 55S ribosomal subunit, mitochondrial, ribosome (80S), ATP synthase, spliceosome A complex, spliceosome E complex, spliceosome C complex, TNF-alpha/NF-kappa B signaling complex, Respiratory chain complex I. These complexes show the relationship between CDS length/ amino acid length and expression.

The CDS length of the gene and amino acid length of the protein are derived from the NCBI-owned CCDS dataset (https://www.ncbi.nlm.nih.gov/projects/ccds/ ccdsbrowse.cgi). R(R-4.3.0) was used to screen the expression levels of protein complexes in different data sets.

**Statistical Analysis**

R(R-4.3.0) package nls2(0.3-4) and ggplot2(3.5.1) were used to analyze and fit the relationship between CDS length/ amino acid length and expression quantity of each database. The absolute abundance of RNA sequencing is used to calculate the FPKM/ RPKM value, and the FPKM/RPKM value is fitted to the absolute abundance of mass spectrometry to check the correlation between data RNA and protein data. The FPKM/RPKM value and absolute abundance of mass spectrometry were fitted with CDS and amino acid length, respectively. The fitting of abundance and length uses a power model. The fitting of RNA FPKM value and protein abundance uses a linear model.

**Results**

**Inverse Correlation Between the mRNA Abundance and CDS Growth**

It has been proposed and demonstrated that their gene length/protein coding sequence (CDS) length limits mRNA levels in nematodes. Considering that synthesized mRNA energy is proportional to length, can mRNA abundance possibly correlate with its CDS length? A variety of brain tissue mRNA sequencing (mRNA-seq) data was collected, including mouse hippocampus single- cell mRNA-seq data, microfluidic isolation of hippocampal axonal mRNA-seq data, mouse hippocampus long-read ONT RNA-seq data, and mouse neocortex bulk RNA-seq data [4-7].

Considering specific energy and protein turnover requirements at the distal axon, the mRNA data of protein complexes, including the mitochondrial ribosomes (55S), ribosomes (80S), ATP synthase, respiratory chain complex I, spliceosome, nuclear pore complexes, and TNF-alpha/NF-kappa B signaling complexes were collected for further analysis. The mRNA FPKM abundance was calculated and plotted against the length of the CDS. The power function was applied under the R language nls2 package. We observed that the mRNA abundance (FPKM) decreases along with the CDS increase (Figure 1A-D). The fitting exhibited correlation coefficients within the range of 0.57 to 0.24, accompanied by exceedingly low P-values. These results show that mRNA FPKM abundance in neural tissues negatively correlates with mRNA length. The longer the mRNA (CDS), the lower the mRNA abundance. This may correlate with the energy consumption required to synthesize the mRNA since the longer the mRNA, the smaller the ribosomal density. This indicates the presence of a mRNA length-dependent control of translation.

In light of the results above, we investigated the applicability within the context of the specified protein complexes. The results for datasets are as follows: mouse Neocortex dataset, mean R2=0.3829 (Figure 1H), long read long ONT sequencing of the hippocampus avg R2=0.525 (Figure 1G), hippocampal 10×snRNA-seq mean R2=0.4586(Figure 1E), and microfluidic harvesting of bulk RNA-seq of neuron axon in hippocampal DG region, mean R2=0.4214(Figure 1F), respectively.

NPC proteins had an inverse correlation between CDS and mRNA abundance in all datasets, and this correlation ranged from 0.20 to 0.46. In contrast, the spliceosome has a lower correlation (R2=0.03~0.15). The TNF complex, respiratory chain complex I and 55S also conformed to the inverse relationship between CDS and mRNA abundance, and the correlations ranged from 0.18~0.97 (TNF), 0.24~0.78 (respiratory chain complex), and 0.18~ 0.43 (55S), respectively. Whereas 80S was expressed as an inverse relationship between CDS and mRNA abundance but with fluctuating slopes in most of the data (R2 = 0.14~0.69), a small portion of the data had the exact low correlation of the spliceosome (R2 = 0.02). There was ambiguity in the ATP synthase results, which conformed to an inverse relationship between CDS and mRNA abundance in the three high correlation data (R2=0.63~0.87) while having a positive relationship between CDS and mRNA abundance in the other data (0.42~0.81). Considering the smaller number of proteins (15 subunits) in ATP synthase, it suggests that the positive relationship between ATP synthase CDS and mRNA abundance results from assay differences. The fitting results show that almost all given complexes correlate with increasing CDS length and decreasing mRNA abundance. The fluctuating slope ranges of many complexes may result in the heterogeneity abundance of protein complex subunits.

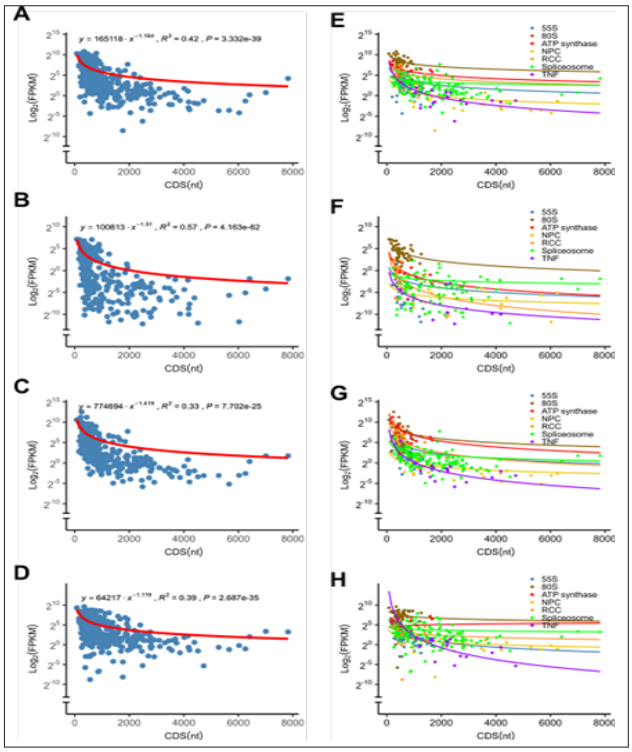


**Figure 1:** Transcriptome Data and the Impact of Gene Length in Nerve Tissues

(A-H) Relationship between the mRNA expression and protein coding sequence (CDS) length. The pooled mRNA abundance of the significant protein complex against CDS was plotted in (A-D), while the mRNA abundance of each protein complex against CDS was plotted in (E-H). Reads Per Kilobase of transcript per Million mapped reads (RPKM). (A, E) The pooled central protein complex mRNA abundance of mouse hippocampus single nucleus mRNA-seq (snRNA-seq) ($R^2$=0.42, P <0.0001), while each protein complex including 55S, $R^2$=0.34; 80S, $R^2$=0.35; ATP synthase, $R^2$=0.63; NPC, $R^2$=0.46; RCC, R2=0.37; spliceosome, $R^2$=0.13; TNF: R2=0.93 in E. (B, F) The pooled main protein complex mRNA abundance of mouse hippocampus DG neuron axonal bulk RNA-seq ($R^2$=0.57, P <0.0001), while each protein complex including 55S, $R^2$=0.27; 80S, $R^2$=0.69; ATP synthase, $R^2$=0.87; NPC, $R^2$=0.23; RCC, $R^2$=0.54; spliceosome, $R^2$=0.11; TNF: $R^2$=0.13 in F. (C, G) The pooled main protein complex mRNA abundance of mouse hippocampus long-read ONT RNA-seq ($R^2$=0.33, P <0.0001),

while each protein complex including 5S, $R^2$=0.37; 80S, R2=0.27; ATP synthase, $R^2$=0.70; NPC, $R^2$=0.42; RCC, $R^2$=0.58; spliceosome, $R^2$=0.14; TNF, $R^2$=0.97 in G. (D, H) The pooled main protein complex mRNA abundance of mouse neocortex bulk RNA-seq (R2=0.33, P<0.0001), while each protein complex including 55S, R2=0.37; 80S, $R^2$=0.27; ATP synthase, $R^2$=0.70; NPC, $R^2$=0.42; RCC, $R^2$=0.58; spliceosome, $R^2$=0.14; TNF, R2=0.97 in H. Abbreviation, 55S ribosome (55S), ATP synthase, nuclear pore protein complex (NPC), respiratory chain complex I (RCC), spliceosome (ACE), TNF-alpha/NF-kappa B signaling complex (TNF), ribosome(80S).

**A Loose Correlation Between Protein Abundance and mRNA FPKM Abundance**

The protein translation rate within a cell is regulated by mRNA abundance. Therefore, we examined the relationship between the protein and mRNA abundance correspondence. Four sets of data from three studies: Bulk RNA-seq and mass spectrometry data generated from parallel the samples of the neocortex in P0 mice and the cerebral cortex in adult humans [7,8]. The other two data sets were produced using the scSTAP technique to obtain the paired snRNA-seq and single-cell proteome data from mouse GV-stage and MII-stage oocytes, respectively, as the reference. The protein abundance mRNA abundance (FPKM) was fitted with the linear function, revealing that the correlation was generally poor [9]. The higher correlation was found in the human cerebral cortex dataset $R^2$= (0.47, P<0.0001) (Figure 2A) followed by the mouse Neocortex dataset ($R^2$=0.15, P=0.0072 correlation (Figure 2B); the dataset of mouse oocyte GV in Figure 2C ($R^2$=0.13, P=0.15), and MII in Figure 2D ($R^2$=0.07, P=0.47). While, the pooled mRNA and protein data from the above-mentioned protein complex show similar low correlation: Human cerebral cortex, $R^2$=0.26, P<0.0001; Mouse neocortex, $R^2$=0.06, P<0.0001; GV, $R^2$=0.15, P<0.0001; MII, $R^2$=0.10, P<0.0001) (Figure 2E-H). These results suggest that some protein complexes have an inverse relationship between mRNA abundance and CDS length in neural tissues. In contrast, the correlation between mRNA and protein abundance in neural tissues is poor. The structure protein abundance is relatively stable, whereas its RNA quantity tends to have a dynamic range. This suggests that mRNA abundance is not always correlated to protein expression.

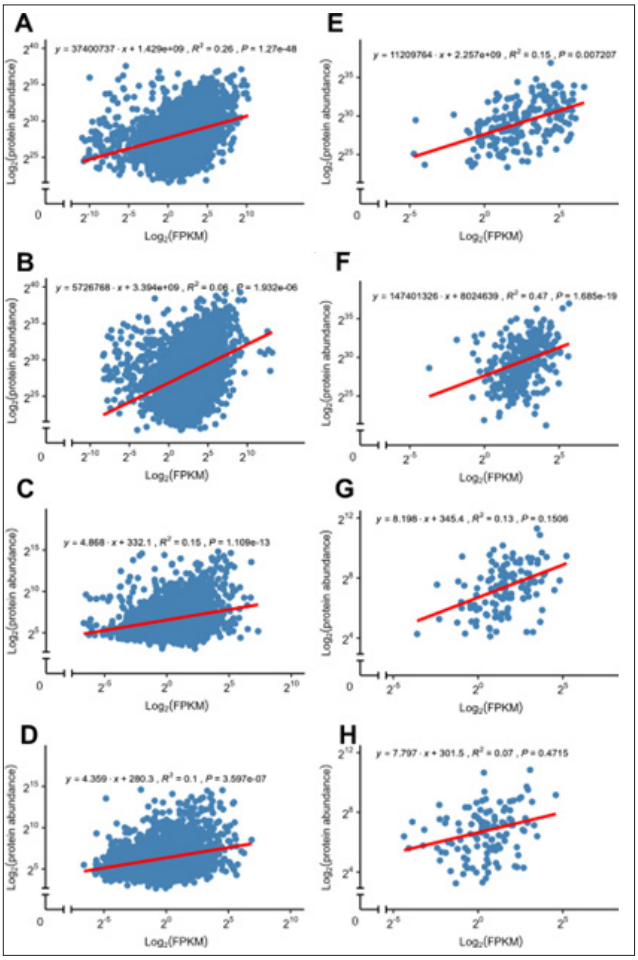


**Figure 2:** Correspondence Between Observed mRNA and Protein Expression. Relationship Between Protein Abundance and RNA-seq Abundance from Paired Measurement

The all-detectable paired mRNA data were pooled and plotted in (A-D), while the paired data of the main protein complex were plotted in (E-H). Reads Per Kilobase of transcript per Million mapped reads (RPKM). (A, E) The data of the P0 mouse neocortex ($R^2$=0.26, P<0.0001), while the pooled major protein complex, $R^2$=0.15, P<0.0001 in E. (B, F) The data of the human cerebral cortex ($R^2$=0.06, P<0.0001), while the pooled major protein complex, $R^2$=0.47, P<0.0001 in F. (C, G). mouse oocyte mRNA at the GV stage ($R^2$=0.15, P=0.007207), while the pooled major protein complex, $R^2$=0.13, P=0.1506 in G. (D, H) mouse oocyte mRNA at the MII stage ($R^2$=0.10, P < 0.0001), while the pooled major protein complex, $R^2$=0.07, P=0.4715 in H.

**The Heterogeneity of the Protein Complexes at mRNA and Protein Abundance**

To study the heterogeneity of protein complexes at RNA and protein levels. Each protein complex from the abovementioned datasets was normalized by one medium- abundance mRNA/protein. The results are visualized in a matrix diagram, in which columns represent data sets, and rows represent the normalized data. At the RNA level, ribosomes, NPC, and respiratory chain complex I all show the heterogeneity ratio of the same mRNA among different data sets, and the heterogeneity level is high. However, some mRNA expressions are stable. The heterogeneity is relatively lower at the protein level than at the RNA level. At the same time, some protein expressions are stable. On both levels, ribosomes have the highest heterogeneity, and NPC and respiratory chain complex I have less heterogeneity than ribosomes. We use a normalized ratio and pay attention to the proportional relationship of different subunits in the protein complex. Heatmap analysis further highlighted distinct signatures in the P0 mouse neocortex and human cerebral cortex as separate clusters (Figure 3D). Employing the differential Ribosome assay, we observed increased stoichiometry of two ribosome proteins and decreased stoichiometry of most ribosome proteins in mature human neurons in comparison to the P0 mouse neuron, while increased stoichiometry of five respiratory chain complex I (NDUFS6, NDUFA5, NDUFV1, NDUFV2, NDUFB3) (Figure 3F) in mature human neurons, and increased stoichiometry of twelve NPC and decreased stoichiometry of only one ribosome proteins in mature human neurons (Figure 3B).

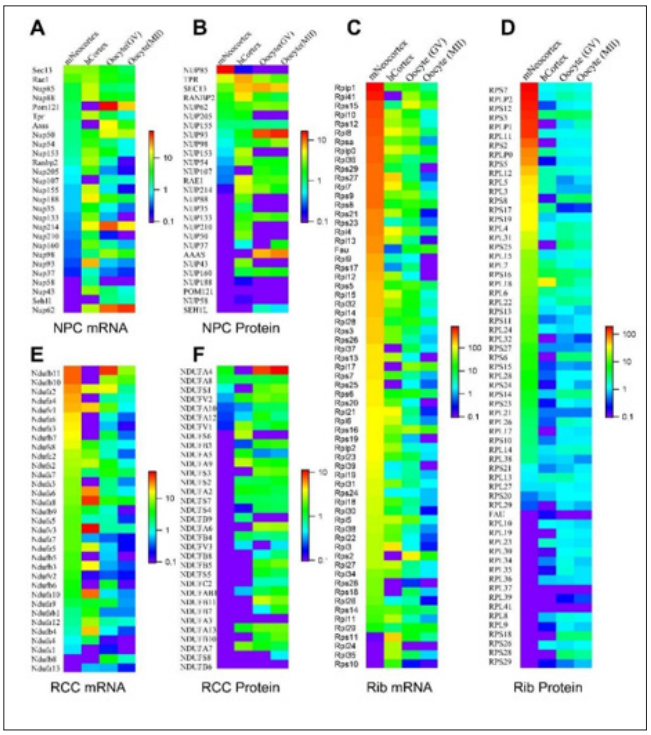


**Figure 3:** Heterogeneity and Stability of Protein Complexes

(A, C and E) Using mRNAseq data sets to visualize the mRNA FPKM abundance, from left to right, P0 mouse neocortex, human cerebral cortex, mouse oocyte mRNA at the GV stage. and MII stage. (B, D, and F) Using paired MS data sets to calculate the relative protein abundance, from left to right, P0 mouse neocortex, human cerebral cortex, mouse oocyte protein at the GV stage, and MII stage. (A) Normalized FPKM abundance for nuclear pore complex. Most complex proteins are heterogeneous, and a few proteins, such as Nup107, Nup210, Nup35, and Nup160, are stable. (B) Nup155(NUP155) was used to normalize the expression ratio of nuclear pore complex protein. Most complexes are heterogeneous, and a few stable proteins, such as Nup107, Nup160, Nup62, and Nup93. (C) Normalized FPKM abundance for ribosome (80S). Most complex proteins are heterogeneous, and a few are stable, such as Rps29, Rpl14, Rpl35, and Rpl27. (D) RPL27(RPL27) was used to normalize the expression ratio of ribosome (80S) protein. Most complex proteins are heterogeneous, and a few are stable, such as Rpl29, Rpl35, Rps29, and Rpl34. (E) Normalized FPKM abundance for respiratory chain complex I. Most complex proteins are heterogeneous, and some are stable, such as Ndufs4, Ndufs1, Ndufa13, and Ndufs7. (F) Ndufa8 (NDUFA8) was used to normalize the expression ratio of respiratory chain complex I protein. Most complex proteins are heterogeneous, but some are stable, such as Ndufc2, Ndufb4, Ndufs7, and Ndufa10.

**Comparison of the Heterogeneity of Ribosome and NPC**

The relatively highly heterogeneous 80S, NPC, and respiratory chain complex I was further studied to get an insight into the heterogeneity of protein complexes. Four single-cell mass spectrometry (scMS) data, including A549, U2OS, HeLa, and HEK293T cell lines, were analyzed to study the heterogeneity of protein complexes. Taking NPC as an example, the protein abundance was normalized by the low abundance protein (NUP107, NUP214) or intermediate abundance protein (NUP155), and the average value and the standard deviation were extracted. The 15 proteins of each cell line with a minor standard deviation representing stable protein were considered the most intergroup-stable proteins.

Then, the intersection of intergroup stable proteins and intragroup stable proteins confirmed the stable, low heterogeneity proteins. Finally, NUP155 was used as a reference to obtain the proportion of stabilized NPC proteins for the three groups of normalized data, which totaled

12 proteins (NUP85, NUP88, NUP188, SEH1L, AAAS, NUP177, etc.). We validated this by calculating ratios using SDS-PAGE data from a previous study and found that SEH1L, NUP205, and NUP214 were similar, validating NPC protein ratio stability (Figure 4B) [10].

Similarly, we used the same approach to obtain the proportion of stable proteins for the 80S, normalized using the lower abundance RPL10 and RPS12 and the intermediate abundance RPL26. By selecting the 30 proteins with the minor standard deviation, we ended up with 22 more stable proteins with low heterogeneity (RPS15, RPS27, RPL36, RPL38, RPL37, RPL32, etc.). However, we did not find suitable data to validate it. We additionally analyzed two protein complexes, mitochondrial ribosomes (55S) and respiratory chain complex I, which showed a small amount of stability in protein abundance and most of the heterogeneity in protein abundance. The SDS-PAGE data was used to verify the quantitative ratios of four out of six (Figure 4D) [10]. Two out of three were consistent (Figure 4C) [11,12].

These results are not in line with the mature NPC protein ratios revealed by STED microscopy, electron microscope (PDB Entry ID: 7R1Y, 7R5J, 7R5K), and mature ribosomes (PDB Entry ID: 5T2C) [13-15]. This suggests that the differences arise from free protein format or different stoichiometry of protein complexes, which may also involve protein turnover of protein complexes. The vast majority of low-heterogeneity ribosomal proteins are at low expression levels. It suggests that these proteins are essential with stable trace expression and, therefore, may have a constant proportion within the ribosome, even in various heterogeneous/stoichiometry ribosomes.

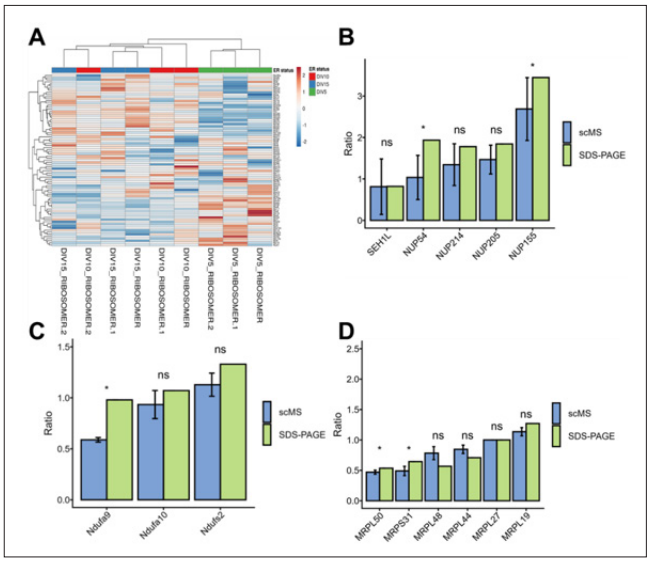


**Figure 4:** Stability of Protein in Different Single-Cell MS Data

(A) Published protein mass spectrometry data from human primary cortical neurons in different periods were used to normalize the total expression of ribosomes and create a heat map [16]. The heat map demonstrates heterogeneity among different samples in the same period. (B) The numerical relationship of the stable NPC protein ratio calculated by taking NUP107 is similar to SDS-PAGE. Blue represents MS data, and green represents reference SDS-PAGE data. The specific protein ratios are: NUP155 (blue: 2.69, green: 3.45), NUP205 (blue: 1.47, green: 1.84), NUP214 (blue: 1.34, green: 1.78), NUP54 (blue: 1.04, green: 1.1). Three of the five genes were not disassembled. (C) The numerical relationship of the stable respiratory chain complex I protein ratio calculated by taking NDUFA13 is similar to SDS-PAGE. Blue represents MS data, and green represents reference SDS-PAGE data. The specific protein ratio is: NDUFA9 (blue: 0.59, green: 0.98), NDUFA10 (blue: 0.93, green: 1.07), N NDUFS2 (blue: 1.13, green: 1ww.33). Two of the three genes were not disassembled. (D) The specific numerical relationship of the stable mitochondrial ribosome (55s) protein ratio calculated by taking MRPL27 is similar to SDS-PAGE. Blue represents MS data, and green represents reference SDS-PAGE data. The specific protein ratios are MRPL27 (blue: 1, green: 1), MRPL44 (blue: 0.85, green: 0.71), MRPL48 (blue: 0.78, green: 0.57), MRPL50 (blue: 0.47, green: 0.54), MRPL19 (blue: 1.14, green: 1.27), MRPS31 (blue: 0.49, green: 0.64), MRPS7 (blue: 2.23, green: 2.02). Four of the six genes were not disassembled.

## Discussion

The inverse relationship between RNA abundance and mRNA length in neural tissue aligns with previous studies on T. brucei. This demonstrates that neurons, although having unique axonal mRNA transport and translation mechanisms, still share a general mechanism. We found that long-read ont mRNA-seq and single-cell mRNA-seq data are more reliable for detecting housekeeping genes within a single cell. In addition, the relationship between RNA and protein has a low correlation, as measured from paired mRNA-seq and proteomic data. A similar tendency was observed in different datasets.

The single-cell mass spectrometry data revealed and verified the relatively stable NPC and ribosome proteins, allowing us to calculate the proportion of each subunit of the given protein complex. The calculated subunit ratio of the given protein complex differs from the proportion of the mature stoichiometry measured by STED microscopy and the protein complex calculated using the Cryo-EM structure data. This demonstrates that the mature protein complex is part of the protein complex's stoichiometry. It is necessary to identify heterogeneous stoichiometry in the future.

## References

1. Jeacock L, J Faria, D Horn (2018) Codon usage bias controls mRNA and protein abundance in trypanosomatids. eLife 7.
2. Genuth NR, M Barna (2018) The Discovery of Ribosome Heterogeneity and Its Implications for Gene Regulation and Organismal Life. Molecular Cell 71: 364-374.
3. Norris K, T Hopes, JL Aspden (2021) Ribosome heterogeneity and specialization in development. WIREs RNA 12.
4. Joglekar A, Wen Hu, Bei Zhang, Oleksandr Narykov, Mark Diekhans, et al. (2023) Single-cell long-read mRNA isoform regulation is pervasive across mammalian brain regions, cell types, and development. bioRxiv 2023.
5. Yang Z, Pengfei Che, Gaoxin Long, Yunxuan Wang, Jaewon Park, et al. (2023) Facilitation of axonal transcriptome analysis with quantitative microfluidic devices. Lab on a Chip 23: 2217-2227.
6. Jones EF, Timothy C Howton, Victoria L Flanary, Amanda D Clark, Brittany N Lasseigne (2024) Long-read RNA sequencing identifies region- and sex-specific C57BL/6J mouse brain mRNA isoform expression and usage. bioRxiv 2024.
7. Harnett D, Ulrike Zinnall, Alexandra Rusanova, Ekaterina Borisova, Amelie N Drescher, et al., (2022) A critical period of translational control during brain development at codon resolution. Nature Structural & Molecular Biology 29: 1277-1290.
8. Eraslan B, Dongxue Wang, Mirjana Gusic, Holger Prokisch, Björn M Hallström, et al. (2019) Quantification and discovery of sequence determinants of protein-per-mRNA amount in 29 human tissues. Molecular Systems Biology 15.
9. Jiang YR, Le Zhu, Lan-Rui Cao, Qiong Wu, Jian Bo Chen, et al. (2023) Simultaneous deep transcriptome and proteome profiling in a single mouse oocyte. Cell Reports 42.
10. Asakawa H, Hui Ju Yang, Takaharu G Yamamoto, Chizuru Ohtsuki, Yuji Chikashige, et al. (2014) Characterization of nuclear pore complex components in fission yeastSchizosaccharomyces pombe. Nucleus 5: 149-162.
11. Matthews DE, R A Hessler, N D Denslow, J S Edwards, T W O'Brien (1982) Protein composition of the bovine mitochondrial ribosome. Journal of Biological Chemistry 257: 8788-8794.
12. Ansari F, Belem Yoval Sánchez, Zoya Niatsetskaya, Sergey Sosunov, Anna Stepanova, et al. (2021) Quantification of NADH: ubiquinone oxidoreductase (complex I) content in biological samples. Journal of Biological Chemistry 297.
13. Otsuka S, Jeremy O B Tempkin, Wanlu Zhang, Antonio Z Politi, Arina Rybina, et al. (2023) A quantitative map of nuclear pore assembly reveals two distinct mechanisms. Nature 613: 575-581.
14. Mosalaganti S, Reiya Taniguchi, Beata Turoňová, Christian E Zimmerli, Katarzyna Buczak, et al. (2022) AI-based structure prediction empowers integrative structural analysis of human nuclear pores. Science 376: eabm9506.
15. Zhang X, Mason Lai, Winston Chang, Iris Yu, Ke Ding, et al. (2016) Structures and stabilization of kinetoplastid-specific split rRNAs revealed by comparing leishmanial and human ribosomes. Nature Communications 7.
16. Gao Y, H Wang (2023) Ribosome Heterogeneity in Development and Disease. bioRxiv 2023.